Research Article Vol. 6, No. 9 / September 2019 / Optica 1110

Microresonator soliton dual-comb imaging

Chengying Bao,[1,†] Myoung-Gyun Suh,[1,2,†] and Kerry Vahala[1,*]

[1]T. J. Watson Laboratory of Applied Physics, California Institute of Technology, Pasadena, California 91125, USA
[2]NTT Physics and Information Laboratory, 1950 University Ave., East Palo Alto, California 94303, USA
*Corresponding author: vahala@caltech.edu

Received 8 April 2019; revised 5 July 2019; accepted 24 July 2019 (Doc. ID 364448); published 27 August 2019

Fast-responding detector arrays are commonly used for imaging rapidly changing scenes. Besides array detectors, a single-pixel detector combined with a broadband optical spectrum can also be used for rapid imaging by mapping the spectrum into a spatial coordinate grid and then rapidly measuring the spectrum. Here, optical frequency combs generated from high-*Q* silica microresonators are used to implement this method. The microcomb is dispersed in two spatial dimensions to measure a test target. The target-encoded spectrum is then measured by multi-heterodyne beating with another microcomb having a slightly different repetition rate, enabling an imaging frame rate up to 200 kHz and fill rates as high as 48 megapixels/s. The system is used to monitor the flow of microparticles in a fluid cell. Microcombs in combination with a monolithic waveguide grating array imager could greatly magnify these results by combining the spatial parallelism of detector arrays with spectral parallelism of optics.

https://doi.org/10.1364/OPTICA.6.001110

1. INTRODUCTION

The development of the rapid-frame-capture detector array sensors based on charge-coupled device and complementary metal oxide semiconductor technology has revolutionized imaging (see, for example, Ref. [1]). Recently, there has also been interest in new methods that leverage the massive bandwidth of optical signals to perform imaging using a single-pixel detector. One such approach uses the broadband spectrum of ultrashort optical pulses [2] and works by mapping different optical frequencies into distinct spatial locations using spatial dispersers such as demonstrated in the technique of femtosecond pulse shaping [3]. To create a two-dimensional (2D) map, a conventional grating disperses the spectrum in one spatial dimension, while a virtually imaged phase array (VIPA) disperses light into the other spatial dimension. As shown in Fig. 1(a), the grating and the VIPA create a "2D spectral shower" in which distinct optical frequencies have a one-to-one (spectral-spatial) correspondence with spatial coordinates in two dimensions [2,4–6]. To recover the image, the spectrum can be measured by the time-stretch method, which converts the spectrally encoded spatial information into a temporal waveform measured on the single-pixel photodetector [2]. This approach measures the image on a shot-by-shot basis and 6 MHz frame rates have been demonstrated [2].

An alternative image recovery technique based on two frequency combs has also been recently demonstrated [6]. This approach, termed here dual-comb imaging, parallels the technique of dual-comb spectroscopy [7,8] by converting an optical spectrum into a radio frequency (RF) electrical signal. In effect the method maps the optical signal comb with target information into these radio frequency components [see Fig. 1(b)]. If the signal and reference comb are phase locked then both amplitude and phase information about the target can be retrieved, enabling acquisition of three-dimensional information [6]. Line-scan spectral-spatial imaging using dual frequency combs has also been recently reported [9–11]. To generate broadband optical pulses for imaging, tabletop mode-locked lasers have so far been used. A recent advance in optical pulse and frequency comb generation is based on dissipative Kerr soliton mode locking in optical microcavities [12–17]. The devices provide high repetition rate soliton streams and their associated optical frequency combs feature smooth spectral envelopes. These miniature frequency combs, or microcombs [18], are considered a possible way to dramatically reduce the form factor of conventional frequency comb systems. Accordingly, they are being studied for several applications including dual-comb spectroscopy [19,20], ranging [21,22], optical communications [23], optical frequency synthesis [24], and exoplanet detection in astronomy [25,26].

The application of microcombs to the dual-comb imaging method is considered here. These devices offer a system-on-a-chip architecture that eliminates fiber optics (i.e., that required for the time-stretch image recovery method and to generate mode-locked pulses). A fully integrated platform that avoids the free space grating and VIPA elements is also possible [see Fig. 1(c)]. This work explores soliton microcomb dual-comb imaging by measuring a USAF1951 test target and by monitoring microparticles in a flow-cell. An important feature of microcombs is their very high repetition rate as compared to conventional combs (typically microwave to terahertz rates as compared to radio frequency rates). The impact of such high repetition rates on future dual-comb imaging system performance is also considered.

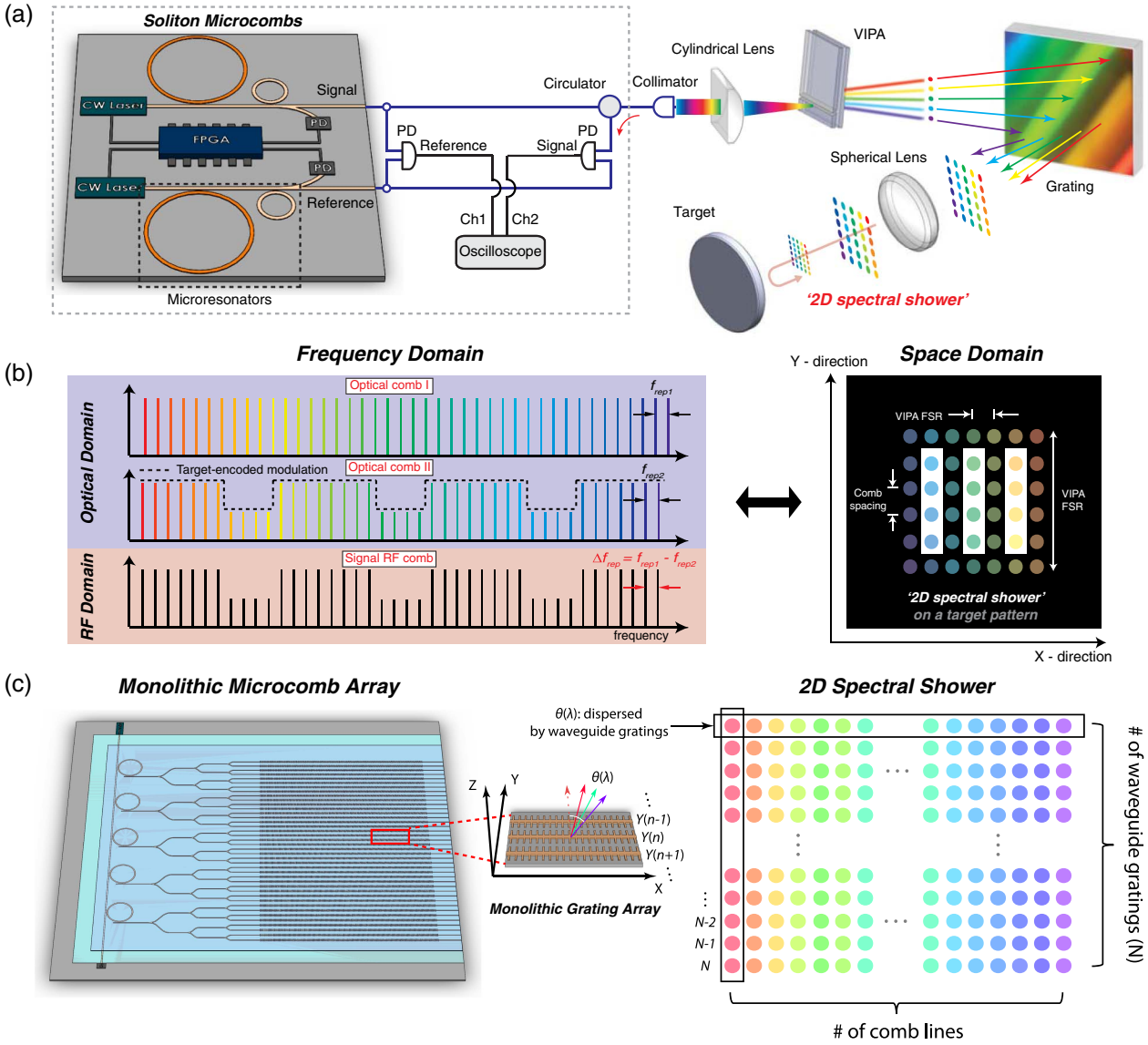

Fig. 1. Dual-comb imaging using microresonator solitons. (a) A conceptual diagram showing the operational principle for spectral-spatial-mapping and dual-microcomb imaging. Two soliton microcombs (signal and reference) having slightly different repetition rates are generated using two on-chip microresonators. A 2D disperser (VIPA+grating) maps frequencies from the signal microcomb into a 2D grid of spatial locations (spectral shower) that are reflected by a target. The reflected signal spectrum is measured by multi-heterodyne detection with the reference microcomb. The chip is shown with small (high rate) and larger (low rate) comb pairs in both the signal and reference arms. These can enable different operational modes for the imaging system. (b) Dual-comb imaging proceeds by illuminating the target (right panel) with the 2D spectral shower formed as shown in panel (a). As shown in the left panel, the target reflection amplitude is encoded onto the signal comb (Optical comb II). The signal comb is then heterodyned with the reference comb (Optical comb I) to generate the RF comb. f_{rep1}, f_{rep2}, and Δf_{rep} are the frequency line spacing of the reference comb, the signal comb, and the signal RF comb. (c) Dual-comb imaging concept based on integrated waveguide grating antennas. Microcomb outputs are divided into multiple waveguides that drive the grating antennas. Comb light is dispersed by a corresponding waveguide grating antenna (eliminates VIPA and grating) to create one imaging dimension in the spectral shower (right). The second imaging dimension is provided by the spatial location of each grating antenna. This approach combines spectral parallelism of photonics with spatial parallelism of detector arrays to greatly magnify performance. A single (shared) pump is shown, but the microcombs could also be individually pumped so as to create frequency combs that are spectrally displaced. Receiver combs and antennas are not shown.

2. EXPERIMENTAL SETUP

High-Q silica-on-silicon wedge microresonators [27] are used to generate the dual soliton streams. The devices feature repetition rates of 1.86 and 9.39 GHz [28]. Details on methods used to trigger and stabilize the soliton microcombs are presented elsewhere [13]. The microcombs are coupled directly to optical fibers using tapered-fiber couplers [29,30]. The signal comb and reference comb are conveyed along the optical train, as shown in Fig. 1(a). The tapered-fiber couplers can be replaced by integrated waveguides [31]. Moreover, fully integrated soliton microcombs with an on-chip pump have also been reported [32].

The VIPA and grating act together to create the 2D spectral shower with the VIPA dispersing the spectrum along the vertical direction and the grating dispersing the spectrum along the horizontal direction. More specifically, the VIPA disperses light only within its free spectral range (FSR), which means that optical

frequencies ν and $\nu + mf_{\mathrm{VIPA}}$ (where m is an integer and f_{VIPA} is the VIPA FSR) will overlap in space. By adding a grating, frequencies ν and $\nu + mf_{\mathrm{VIPA}}$ can be further dispersed to create the 2D spectral shower, as illustrated in Figs. 1(a) and 1(b). The VIPA used in our experiment has an FSR of 60 GHz (LightMachinery) and this limits pixel count along the vertical direction to 6 pixels (9.39 GHz microcomb) and 32 pixels (1.86 GHz microcomb). Analysis of more optimal designs is provided in the Discussion. The spectral shower is reflected by the object, coupled back into the fiber for return to a photodetector where it is heterodyned with the reference microcomb. Figure 1(b) illustrates how the image reflection amplitude is transferred from the spectral shower to the signal RF spectrum produced by dual-comb heterodyne.

Also shown in Fig. 1(a) are a collimator and a cylindrical lens (focal length of 150 mm) that focuses the collimated comb onto the VIPA. Additionally, the 2D spectral shower is focused onto the target by a spherical lens (focal length of 30 mm). The targets are placed at the focal plane of the spherical lens and aligned to provide maximum reflection coupled into the fiber. Because the dual-comb measurement can resolve single comb lines, the spatial resolution is set by the imaging system only. This is in contrast to the time-stretch method where spatial resolution can also be limited by the ability to resolve the frequency components [2]. The spot diameter of a dispersed comb line is ~15 μm in the current setup and a finer spot size can be achieved by expanding the beam size before the focusing spherical lens.

3. IMAGING A STATIC TARGET

To demonstrate this approach, a USAF 1951 test target (negative) is imaged. In a first measurement, two independent free-running silica microcombs with repetition rates close to 9.39 GHz are used. Dual combs can also be generated from a single microresonator [33–35], which can result in strong common noise

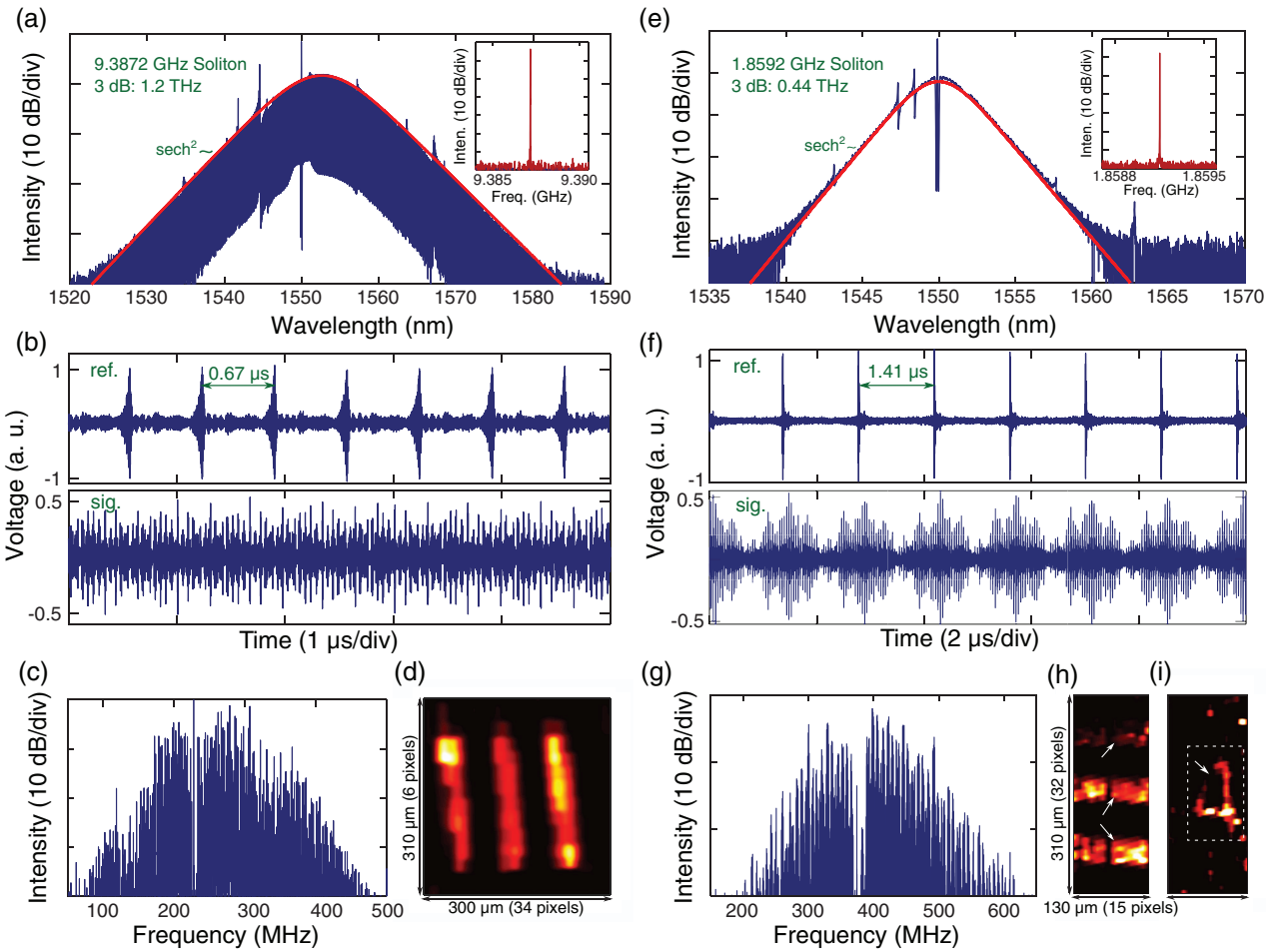

Fig. 2. Dual-microcomb imaging of static targets. (a) Typical optical spectrum of the 9.39 GHz soliton microcombs showing sech^2 spectral envelope fit (red) with 3 dB bandwidth of 1.2 THz. The inset is the electrical spectrum of the photodetected soliton pulse stream and gives the repetition rate. (b) An example of the measured interferogram in a 5 μs time window from the reference arm and the signal arm [see Fig. 1(a)]. (c) RF spectrum of the 5 μs signal interferogram in panel (b). (d) Image of three vertical bars constructed from the measured interferogram in panel (b). (e) Typical optical spectrum of the 1.86 GHz soliton microcombs showing sech^2 spectral envelope fit (red) with 3 dB bandwidth of 0.44 THz. A notch near the spectral maximum is produced by narrowband filtering of the optical pump. The inset is the electrical spectrum of the photodetected soliton pulse stream. (f) Examples of the recorded interferograms for reference and signal arms using the 1.86 GHz microcombs. (g) RF spectrum of the signal interferogram in panel (f). The spectral hole around 380 MHz results from the notch filter used to suppress the optical pump. (h) Image of three horizontal bars constructed from the measured 10 μs interferogram in panel (f). (i) Image of number "4" on the USAF target produced using the 1.86 GHz microcombs. The dark discontinuities shown by the arrows in panels (h), (i) result from the spectral notch produced by filtering the optical pump [see panel (e)]. As an aside, a similar discontinuity is located within a dark region of the image in panel (d) and is therefore not visible.

suppression but it also limits the freedom of choosing the repetition rate difference. Therefore, two independent microresonators were used. The spectrum of one of the microcombs is shown in Fig. 2(a) and features a sech^2-shaped spectral envelope and 3 dB bandwidth of 1.2 THz. The spectral spurs in the spectrum result from the dispersive wave emission induced by avoided mode crossings, which also assists single soliton generation [36]. The detected electrical spectrum for this comb is shown in the inset of Fig. 2(a). The other microcomb has a similar spectrum, but its repetition rate differs from the first microcomb by $\Delta f_{rep} \sim$ 1.5 MHz. The repetition rate difference was chosen to maintain the interferogram bandwidth within the 1 GHz bandwidth of the digitizer used in the experiment. The close matching in the selected repetition rates is possible by good microfabrication control of the resonator diameters using a common mask size and calibration of etch rates [27]. In Fig. 2(b), typical examples of the heterodyned dual-comb interferograms measured over a 5 μs interval from the reference arm (upper panel) and signal arm (lower panel) are shown. While the reference interferogram contains a readily identifiable periodic signal resulting from the difference in repetition rates of the signal and reference microcombs, the signal interferogram contains a complex structure associated with the image.

To construct an image, an RF spectrum is first calculated by taking the fast Fourier transform (FFT) of the signal interferogram produced by illuminating a patterned region of the target [Fig. 2(c)]. Even though free-running microcombs were used, the signal-to-noise ratio is at least 10 dB over most of the spectrum and exceeds 30 dB over a substantial fraction of the spectrum. Furthermore, the RF spectrum is compressed into a bandwidth less than 400 MHz. The signal spectrum is then normalized using the FFT of the reference interferogram. Following this calculation, the same procedure is applied except using a non-patterned (uniform) region of the target. Finally, this non-patterned RF spectrum is used to normalize the RF spectrum of the patterned region, and the resulting normalized spectrum is sorted into the 2D image matrix with each column containing one VIPA FSR. An example of the constructed image is shown in Fig. 2(d).

The low pixel number (~6 × 34) limits the resolution of the image, especially along the vertical direction, which is set by the combination of the 9.39 GHz microcombs with the fixed VIPA FSR. To illustrate possible improvement in the vertical direction, two 1.86 GHz soliton microcombs ($\Delta f_{rep} = 0.7$ MHz) were also tested in the imaging setup [see Fig. 2(e) for the optical and electrical spectra of one of the microcombs]. The pixel number using the 1.86 GHz microcombs is ~15 × 32. The field of view is smaller than the 9.39 GHz microcombs due to the narrower comb bandwidth. Reference and signal dual-comb interferograms can be obtained as before [Fig. 2(f)] with a corresponding signal FFT [Fig. 2(g)]. Figures 2(h) and 2(i) show the resulting images of three horizontal bars and the number "4" (test target), respectively. Figures 2(h) and 2(i) are recorded within a time interval of 10 μs.

As an aside and as noted earlier, locking of the signal and reference combs can allow for phase retrieval enabling three-dimensional imaging similar to [6]. Such locking could also leverage the mutual locking of counter-propagating solitons [33]; however, this will lower the frame rate due to the relatively small repetition rate difference in counter-propagating solitons. Also, even though the 9.39 GHz microcombs and 1.86 GHz microcombs were generated from different chips in the current experiments, multiple comb pairs can be integrated on a single chip to enable agile switching between different operating modes [see Fig. 1(a) for the concept].

4. MONITORING A FLOWING MICROPARTICLE

To demonstrate measurement of a rapidly changing scene, two 9.39 GHz soliton microcombs are used to monitor a microparticle moving in a high-speed flow-cell [Fig. 3(a)]. For this purpose a ~0.25 m/s laminar flow-cell (cross section 0.2 mm × 8 mm) was set up and microparticles with a diameter of ~100 μm

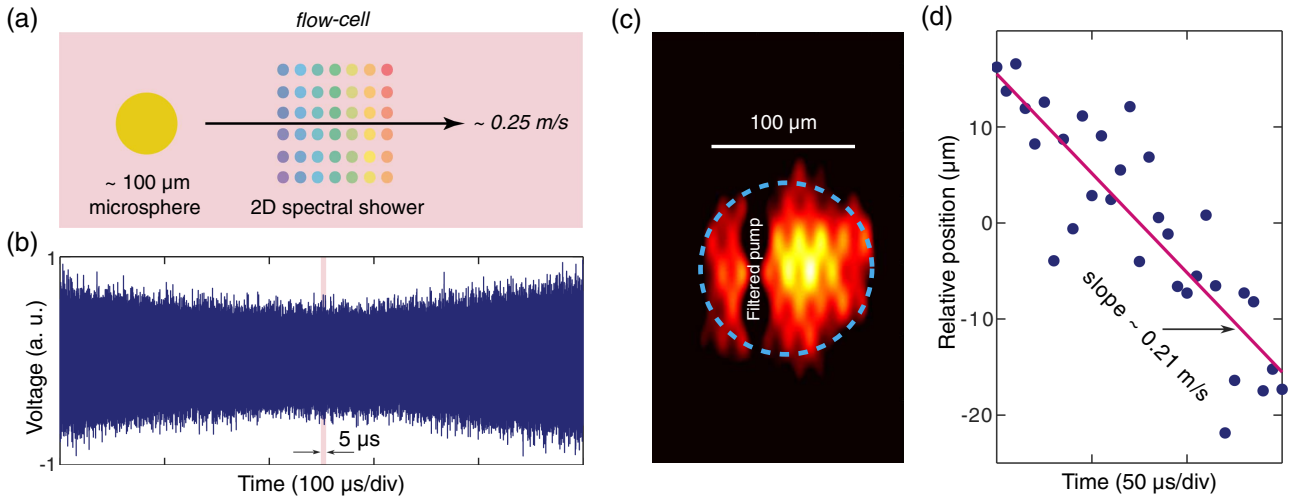

Fig. 3. Monitoring flowing particles. (a) An illustration of the microparticle monitoring experiment. Microparticles are suspended in water and flow inside the cell. When a particle passes through the 2D spectral shower, the particle can be imaged using the dual-comb interferogram. (b) Measured interferogram shows varying amplitude when the microparticle flows through the 2D spectral shower. (c) A snapshot of the measured microparticle, which is constructed from a 5 μs duration interferogram [shaded bar in panel (b)]. The dashed circle suggests the microparticle size (~100 μm). The dark vertical band results from filtering of comb lines around the pump. (d) Center position of the microparticle plotted versus time. A linear fit gives a flow velocity of 0.21 m/s in reasonable agreement with the set water flow velocity of 0.25 m/s.

Table 1. Toward Optimal Design of Dual-Microcomb Imaging Systems

	VIPA FSR	Comb Bandwidth[a]	Δf_{rep}	Frame Rate	Pixels	Fill Rate
100 MHz fiber lasers [6]	15 GHz	1.2 THz	1.2 kHz	1.2 kHz (12 Hz)[b]	12,382	15 (0.15) megapixels/s
9.4 GHz microcombs	60 GHz	1.8 THz	1.5 MHz	200 kHz	204	40 megapixels/s
1.9 GHz microcombs	60 GHz	0.9 THz	0.7 MHz	100 kHz	480	48 megapixels/s
Possible 10 GHz microcombs	500 GHz	25 THz	2 MHz	400 kHz[c]	2500	1 gigapixels/s
100 GHz microcomb array[d]	N/A	10 THz	500 MHz	100 MHz[c]	10,000	1 terapixels/s

[a]This is the comb bandwidth that is available for the image retrieval and can be greater than the 3 dB bandwidth.
[b]The 1.2 kHz frame rate for [6] uses a single period of the interferogram which could limit the image quality. Another frame rate (12 Hz) averages 100 periods and was also reported in [6].
[c]In the current work, averaging over five periods of the interferogram is assumed.
[d]The array consists of 10 signal microcombs with a 10:1 waveguide grating antenna fan-out.

were suspended in water to flow through the cell. To improve signal-to-noise a mirror was placed behind the cell. When a microparticle passes through the spectral shower, it modulates lines in the spectral shower, which results in the amplitude varying interferogram shown in Fig. 3(b). An image of a recorded flowing microparticle is constructed from the 5 μs portion of the interferogram (shaded bar) in Fig. 3(b) and is shown in Fig. 3(c). The size of the reconstructed microparticle (dashed circle in figure) is consistent with the particle's actual size. The particles are not well resolved on account of the limited pixel number. To measure the motion of the microparticle, its center position is plotted versus time in Fig. 3(d). A linear fit gives a flow velocity of 0.21 m/s, consistent with the flow-cell set-point velocity of 0.25 m/s. A 200 kHz frame rate was used in this measurement and ∼7 frames of the heterodyne interferogram were averaged to produce the image. A comparison of frame rate, pixel count, and fill rate for this result versus work using fiber lasers [6] is provided in Table 1.

5. DISCUSSION AND OUTLOOK

A. Repetition Rate and Imaging Performance

Comb repetition rate affects pixel count, fill rate, and frame rate in the dual-comb imaging system. Pixel count determines target resolution and is equal to the number of comb lines:

$$M_1 \times M_2 = B/f_{rep}, \tag{1}$$

where M_1 and M_2 are the pixel count along the two axes of the spectral shower, B is the comb bandwidth, and f_{rep} is the comb repetition rate.

Beyond pixel count, the image processing rate is also important. To better understand the constraints inherent in the dual-comb approach, note that the $M_1 \times M_2$ comb line pixels, once mapped into the radio frequency domain, must fit within a radio frequency bandwidth that is less than $f_{rep}/2$. If this condition is not satisfied, then the optical to radio frequency mapping would result in spectral folding of comb components [7]. This constraint gives $M_1 \times M_2 \times \Delta f_{rep} < f_{rep}/2$. The rate Δf_{rep} also sets the maximum frame rate of the imaging system. This can be understood by considering the interference of the signal and reference combs in the time domain where their different repetition rates cause the combs to strobe one another on the photodetector. Each strobed signal in the detected current contains the complete image information so that the strobing rate (i.e., Δf_{rep}) is the maximum image frame rate. In practice, several strobe periods (C periods) must be averaged to improve the signal-to-noise so that the practical frame rate is $f_{frame} = \Delta f_{rep}/C$. As a result of this relationship, the number of pixels that can be detected per second by the dual-comb imaging system is given by

$$F_1 \equiv M_1 \times M_2 \times f_{frame} = f_{rep}/(2C), \tag{2}$$

where F_1 is the fill rate (pixels per second) of a VIPA + grating imager in Fig. 1(a) or a single waveguide antenna in Fig. 1(c). The fill rate is widely used to characterize video cards, but here it is used to assess the combined space and time resolution of the dual-comb imaging system. Finally, it is also possible to eliminate $M_1 \times M_2$ in the above expression to arrive at

$$f_{frame} < f_{rep}^2/(2\mathrm{BC}). \tag{3}$$

In summary, Eqs. (1)–(3) show that even while the high repetition rates of microcombs degrade space resolution by reduction of pixel count, they simultaneously improve the frame rates and fill rate of the dual-comb imaging system. Indeed, the fill rates of the current demonstrations are higher than fiber laser-based systems (see Table 1). Moreover, as discussed in the next section, it is possible to restore pixel count by combining the spatial parallelism of conventional detector arrays with the spectral parallelism of single-pixel photonic imaging as illustrated in Fig. 1(c).

B. Design Comparisons

For the current VIPA + grating-based system, the assignment of spectral shower pixels to horizontal and vertical axes is controlled through the VIPA FSR (f_{VIPA}) such that $M_1 = f_{VIPA}/f_{rep}$ and $M_2 = B/f_{VIPA}$. As examples, a 25 THz comb bandwidth would enable a horizontal pixel number of 50 using a 500 GHz VIPA (custom design available at LightMachinery). For the vertical direction, the pixel number could be increased to over 50 using 10 GHz repetition rate microcombs. This configuration would provide 2500 pixels at a fill rate of 1 gigapixels/s (see Table 1).

It is also possible to eliminate the discrete VIPA and grating components shown in Fig. 1(a) using the architecture in Fig. 1(c) so that the imaging system (with the exception lenses) can be monolithically integrated. In this design, a waveguide splitter allows fan-out of a single comb into multiple waveguide grating emitters and thereby multiplies pixel count and fill rate by the fan-out number N (i.e., $F_N = NF_1$). The chip-based nature of microcombs can be further leveraged here to implement a monolithic microcomb array [as shown in Fig. 1(c)] to provide additional multiplication of the pixel count in cases where fan-out might be limited on account of comb power. For example, by using an array of 100 waveguide elements driven by ten, 100 GHz repetition-rate microcombs (fan-out of 10:1 for each microcomb) a fill rate of 1 terapixels/s is possible with 10,000 pixels (see Table 1). 100 GHz microcombs can be generated from

silica microresonators with a diameter of ~600 μm or silicon nitride microresonators with a diameter of ~400 μm. Thus, 10 microcombs may be accommodated using less than 1 cm along one linear dimension. On-chip grating antenna arrays have been used for beam steering and Lidar [37]. Different from beam steering, the antennas in the present application can be well separated. The spectral shower can be focused on the imaging target by two orthogonal cylindrical lenses, similar to the control of the dispersed beams in [4]. Then, the encoded spectral shower can be either transmitted or reflected to another receiver photonic chip with a receiver antenna array, a reference microcomb array, and a photodetector array for dual-microcomb heterodyne and image retrieval. In principle, the reference microcomb array and the detector array can be integrated on the same chip with the signal microcomb array. Overall, such a design of monolithic microcombs and grating antennas could be used to resolve transient scenes with excellent space and time resolution.

As an aside, achieving wide comb bandwidth at higher repetition rates using microcombs is straightforward (e.g., 100 GHz microcombs in the fifth row design in Table 1). However, wider bandwidth operation at reduced rates (e.g., 10 GHz microcombs in the fourth row design in Table 1) is more challenging on account of the way continuous-wave pumping efficiency scales with repetition rate [13,38]. However, pulsed pumping can be used to improve pumping efficiency and bandwidth [39]. For example, a 28 GHz microcomb spanning 60 THz has been demonstrated using pulse pumping [40]. External (chip-based) broadeners have also been used to achieve octave-span spectral coverage for 15 GHz microcombs [41].

6. CONCLUSION

In conclusion, soliton microcombs have been applied to image static and moving targets, thereby validating the feasibility of using microcombs for dual-comb imaging. Further integration of microcombs with fan-out waveguide grating arrays and integrated detector arrays would improve fill rate performance and image resolution. This direction of work would leverage both the spatial parallelism of conventional imaging arrays and the spectral parallelism of single-pixel optical imaging. Such systems can also eliminate discrete VIPA and grating components by bringing these functions onto the compact imaging chip. The current demonstration was in the 1.55 μm band, but can be readily shifted to the 1 μm band, which could be more suitable for biological applications [42,43]. The method can potentially find widespread applications in fundamental science as well as in industrial production.

Funding. Air Force Office of Scientific Research (FA9550-18-1-0353); Resnick Sustainability Institute for Science, Energy and Sustainability, California Institute of Technology.

Acknowledgment. The authors thank Taeyoon Jeon and Chengmingyue Li for helpful discussions on the flow-cell experiment. C. B. gratefully acknowledges support from a Postdoctoral Fellowship from the Resnick Institute at Caltech.

†These authors contributed equally to this work.

REFERENCES

1. Y. Kondo, K. Takubo, H. Tominaga, R. Hirose, N. Tokuoka, Y. Kawaguchi, Y. Takaie, A. Ozaki, S. Nakaya, F. Yano, and T. Daigen, "Development of 'hypervision hpv-x' high-speed video camera," Shimadzu Rev. **69**, 285–291 (2012).
2. K. Goda, K. Tsia, and B. Jalali, "Serial time-encoded amplified imaging for real-time observation of fast dynamic phenomena," Nature **458**, 1145–1149 (2009).
3. A. M. Weiner, "Femtosecond pulse shaping using spatial light modulators," Rev. Sci. Instrum. **71**, 1929–1960 (2000).
4. V. Supradeepa, C.-B. Huang, D. E. Leaird, and A. M. Weiner, "Femtosecond pulse shaping in two dimensions: towards higher complexity optical waveforms," Opt. Express **16**, 11878–11887 (2008).
5. S. A. Diddams, L. Hollberg, and V. Mbele, "Molecular fingerprinting with the resolved modes of a femtosecond laser frequency comb," Nature **445**, 627–630 (2007).
6. E. Hase, T. Minamikawa, T. Mizuno, S. Miyamoto, R. Ichikawa, Y.-D. Hsieh, K. Shibuya, K. Sato, Y. Nakajima, A. Asahara, K. Minoshima, Y. Mizutani, T. Iwata, H. Yamamoto, and T. Yasui, "Scan-less confocal phase imaging based on dual-comb microscopy," Optica **5**, 634–643 (2018).
7. I. Coddington, N. Newbury, and W. Swann, "Dual-comb spectroscopy," Optica **3**, 414–426 (2016).
8. N. Picqué and T. W. Hänsch, "Frequency comb spectroscopy," Nat. Photonics **13**, 149–157 (2019).
9. C. Wang, Z. Deng, C. Gu, Y. Liu, D. Luo, Z. Zhu, W. Li, and H. Zeng, "Line-scan spectrum-encoded imaging by dual-comb interferometry," Opt. Lett. **43**, 1606–1609 (2018).
10. X. Dong, X. Zhou, J. Kang, L. Chen, Z. Lei, C. Zhang, K. K. Wong, and X. Zhang, "Ultrafast time-stretch microscopy based on dual-comb asynchronous optical sampling," Opt. Lett. **43**, 2118–2121 (2018).
11. E. Hase, T. Minamikawa, S. Miyamoto, R. Ichikawa, Y.-D. Hsieh, Y. Mizutani, T. Iwata, H. Yamamoto, and T. Yasui, "Scan-less, kilo-pixel, line-field confocal phase imaging with spectrally encoded dual-comb microscopy," IEEE J. Sel. Top. Quantum Electron. **25**, 6801408 (2019).
12. T. Herr, V. Brasch, J. D. Jost, C. Y. Wang, N. M. Kondratiev, M. L. Gorodetsky, and T. J. Kippenberg, "Temporal solitons in optical microresonators," Nat. Photonics **8**, 145–152 (2014).
13. X. Yi, Q.-F. Yang, K. Y. Yang, M.-G. Suh, and K. Vahala, "Soliton frequency comb at microwave rates in a high-Q silica microresonator," Optica **2**, 1078–1085 (2015).
14. C. Joshi, J. K. Jang, K. Luke, X. Ji, S. A. Miller, A. Klenner, Y. Okawachi, M. Lipson, and A. L. Gaeta, "Thermally controlled comb generation and soliton modelocking in microresonators," Opt. Lett. **41**, 2565–2568 (2016).
15. P.-H. Wang, J. A. Jaramillo-Villegas, Y. Xuan, X. Xue, C. Bao, D. E. Leaird, M. Qi, and A. M. Weiner, "Intracavity characterization of micro-comb generation in the single-soliton regime," Opt. Express **24**, 10890–10897 (2016).
16. T. J. Kippenberg, A. L. Gaeta, M. Lipson, and M. L. Gorodetsky, "Dissipative Kerr solitons in optical microresonators," Science **361**, eaan8083 (2018).
17. A. L. Gaeta, M. Lipson, and T. J. Kippenberg, "Photonic-chip-based frequency combs," Nat. Photonics **13**, 158–169 (2019).
18. T. J. Kippenberg, R. Holzwarth, and S. A. Diddams, "Microresonator-based optical frequency combs," Science **332**, 555–559 (2011).
19. M.-G. Suh, Q.-F. Yang, K. Y. Yang, X. Yi, and K. J. Vahala, "Microresonator soliton dual-comb spectroscopy," Science **354**, 600–603 (2016).
20. A. Dutt, C. Joshi, X. Ji, J. Cardenas, Y. Okawachi, K. Luke, A. L. Gaeta, and M. Lipson, "On-chip dual-comb source for spectroscopy," Sci. Adv. **4**, e1701858 (2018).
21. M.-G. Suh and K. J. Vahala, "Soliton microcomb range measurement," Science **359**, 884–887 (2018).
22. P. Trocha, M. Karpov, D. Ganin, M. H. Pfeiffer, A. Kordts, S. Wolf, J. Krockenberger, P. Marin-Palomo, C. Weimann, S. Randel, W. Freude, T. J. Kippenberg, and C. Koos, "Ultrafast optical ranging using microresonator soliton frequency combs," Science **359**, 887–891 (2018).
23. P. Marin-Palomo, J. N. Kemal, M. Karpov, A. Kordts, J. Pfeifle, M. H. Pfeiffer, P. Trocha, S. Wolf, V. Brasch, M. H. Anderson, R. Rosenberger, K. Vijayan, W. Freude, T. J. Kippenberg, and C. Koos,

"Microresonator-based solitons for massively parallel coherent optical communications," Nature **546**, 274–279 (2017).
24. D. T. Spencer, T. Drake, T. C. Briles, J. Stone, L. C. Sinclair, C. Fredrick, Q. Li, D. Westly, B. R. Ilic, A. Bluestone, N. Volet, T. Komljenovic, L. Chang, S. H. Lee, D. Y. Oh, M.-G. Suh, K. Y. Yang, M. H. Pfeiffer, T. J. Kippenberg, E. Norberg, K. Vahala, K. A. Srinivasan, N. R. Newbury, L. Theogarajan, J. E. Bowers, S. A. Diddams, and S. B. Papp, "An integrated-photonics optical-frequency synthesizer," Nature **557**, 81–89 (2018).
25. E. Obrzud, M. Rainer, A. Harutyunyan, M. H. Anderson, J. Liu, M. Geiselmann, B. Chazelas, S. Kundermann, S. Lecomte, M. Cecconi, A. Ghedina, E. Molinari, F. Pepe, F. Wildi, F. Bouchy, T. J. Kippenberg, and T. Herr, "A microphotonic astrocomb," Nat. Photonics **13**, 31–39 (2019).
26. M.-G. Suh, X. Yi, Y.-H. Lai, S. Leifer, I. S. Grudinin, G. Vasisht, E. C. Martin, M. P. Fitzgerald, G. Doppmann, J. Wang, D. Mawet, S. B. Papp, S. A. Diddams, C. Beichman, and K. Vahala, "Searching for exoplanets using a microresonator astrocomb," Nat. Photonics **13**, 25–30 (2019).
27. H. Lee, T. Chen, J. Li, K. Y. Yang, S. Jeon, O. Painter, and K. J. Vahala, "Chemically etched ultrahigh-Q wedge-resonator on a silicon chip," Nat. Photonics **6**, 369–373 (2012).
28. M.-G. Suh and K. Vahala, "Gigahertz-repetition-rate soliton microcombs," Optica **5**, 65–66 (2018).
29. M. Cai, O. Painter, and K. J. Vahala, "Observation of critical coupling in a fiber taper to a silica-microsphere whispering-gallery mode system," Phys. Rev. Lett. **85**, 74–77 (2000).
30. S. M. Spillane, T. J. Kippenberg, O. J. Painter, and K. J. Vahala, "Ideality in a fiber-taper-coupled microresonator system for application to cavity quantum electrodynamics," Phys. Rev. Lett. **91**, 043902 (2003).
31. K. Y. Yang, D. Y. Oh, S. H. Lee, Q.-F. Yang, X. Yi, B. Shen, H. Wang, and K. Vahala, "Bridging ultrahigh-Q devices and photonic circuits," Nat. Photonics **12**, 297–302 (2018).
32. B. Stern, X. Ji, Y. Okawachi, A. L. Gaeta, and M. Lipson, "Battery-operated integrated frequency comb generator," Nature **562**, 401–405 (2018).
33. Q.-F. Yang, X. Yi, K. Y. Yang, and K. Vahala, "Counter-propagating solitons in microresonators," Nat. Photonics **11**, 560–564 (2017).
34. C. Joshi, A. Klenner, Y. Okawachi, M. Yu, K. Luke, X. Ji, M. Lipson, and A. L. Gaeta, "Counter-rotating cavity solitons in a silicon nitride microresonator," Opt. Lett. **43**, 547–550 (2018).
35. E. Lucas, G. Lihachev, R. Bouchand, N. G. Pavlov, A. S. Raja, M. Karpov, M. L. Gorodetsky, and T. J. Kippenberg, "Spatial multiplexing of soliton microcombs," Nat. Photonics **12**, 699–705 (2018).
36. C. Bao, Y. Xuan, D. E. Leaird, S. Wabnitz, M. Qi, and A. M. Weiner, "Spatial mode-interaction induced single soliton generation in microresonators," Optica **4**, 1011–1015 (2017).
37. J. Sun, E. Timurdogan, A. Yaacobi, E. S. Hosseini, and M. R. Watts, "Large-scale nanophotonic phased array," Nature **493**, 195–199 (2013).
38. X. Yi, Q.-F. Yang, K. Y. Yang, and K. Vahala, "Theory and measurement of the soliton self-frequency shift and efficiency in optical microcavities," Opt. Lett. **41**, 3419–3422 (2016).
39. E. Obrzud, S. Lecomte, and T. Herr, "Temporal solitons in microresonators driven by optical pulses," Nat. Photonics **11**, 600–607 (2017).
40. M. Anderson, R. Bouchand, E. Obrzud, J. Liu, S. Karlen, S. Lecomte, T. Herr, and T. J. Kippenberg, "Broadband efficient soliton microcombs in pulse-driven photonic microresonators," in *CLEO: Science and Innovations* (Optical Society of America, 2019), paper STu3J–3.
41. E. S. Lamb, D. R. Carlson, D. D. Hickstein, J. R. Stone, S. A. Diddams, and S. B. Papp, "Optical-frequency measurements with a Kerr microcomb and photonic-chip supercontinuum," Phys. Rev. Appl. **9**, 024030 (2018).
42. S. H. Lee, D. Y. Oh, Q.-F. Yang, B. Shen, H. Wang, K. Y. Yang, Y.-H. Lai, X. Yi, X. Li, and K. Vahala, "Towards visible soliton microcomb generation," Nat. Commun. **8**, 1295 (2017).
43. M. Karpov, M. H. Pfeiffer, J. Liu, A. Lukashchuk, and T. J. Kippenberg, "Photonic chip-based soliton frequency combs covering the biological imaging window," Nat. Commun. **9**, 1146 (2018).